

LOGOS-CA: A Cellular Automaton Using Natural Language as State and Rule

Keishu Utimula
 (Dated: February 12, 2026)

Large Language Models (LLMs), trained solely on massive text data, have achieved high performance on the Winograd Schema Challenge (WSC), a benchmark proposed to measure commonsense knowledge and reasoning abilities about the real world. This suggests that the language produced by humanity describes a significant portion of the world with considerable nuance. In this study, we attempt to harness the high expressive power of language within cellular automata. Specifically, we express cell states and rules in natural language and delegate their updates to an LLM. Through this approach, cellular automata can transcend the constraints of merely numerical states and fixed rules, providing us with a richer platform for simulation. Here, we propose LOGOS-CA (Language Oriented Grid Of Statements – Cellular Automaton) as a natural framework to achieve this and examine its capabilities. We confirmed that LOGOS-CA successfully performs simple forest fire simulations and also serves as an intriguing subject for investigation from an Artificial Life (ALife) perspective. In this paper, we report the results of these experiments and discuss directions for future research using LOGOS-CA.

I. INTRODUCTION

For every known phenomenon, attempts have been made to describe it through “language.” Here, let us take this “language” to include numbers, symbols, and the mathematical equations that combine them. In *Course in General Linguistics*, Saussure argued that language is not merely a label but an arbitrary association between a sound-image and a concept, and further suggested a view of language as a system that carves out phenomena [1]. On the other hand, the early Wittgenstein stated that the world is the totality of facts and that propositions are pictures of facts [2], while in his later work he positioned the act of describing the world as one form of “language-games.” [3] It can be argued that humanity has refined this craft each time it encounters unknown phenomena.

Prior to the emergence of Large Language Models (LLMs), in the context of classical symbolic AI, it was widely believed that an explicit world model was required for AI to understand the real world [4, 5]. The Winograd Schema Challenge (WSC) is one of the most representative benchmarks proposed to measure commonsense knowledge and reasoning abilities about the real world [6]. The authors designed it as a problem that cannot be solved simply through a large corpus and statistical processing on it, and it has been used to investigate AI’s understanding of the real world [6, 7]. However, Trinh and Le showed that an RNN-based language model trained on massive text data in an unsupervised manner achieved 63.7% accuracy on the WSC [8]. Subsequently, GPT-2 improved its score within the same framework, and the following fine-tuned BERT achieved 90% accuracy [7, 9, 10]. These results do not immediately negate the necessity of a world model for the WSC; indeed, some argue that an implicit world model is constructed internally within LLMs [11–13]. In any case, these results suggest that the language humanity has produced captures a significant portion of the world with considerable nuance.

The expressive power of language is unfathomable.

Here, we consider combining the high expressive power of language with cellular automata.

A cellular automaton is a discrete computational model defined by a lattice of cells, each holding a state, and rules governing their updates [14]. This was introduced by John von Neumann as a theoretical framework for discussing self-replicating machines [15–18]. Typically, a cell’s state is one of several integers, and the rules are expressed as program code.

Cellular automata have been used for dynamical system computations including fluid dynamics [19–21], simulations of natural phenomena such as forest fires [22–24], analysis of macroscopic phenomena such as traffic congestion and urban development [25, 26], and even certain types of cryptography [27]. In such applications, cell states are no longer limited to integers; they may also be real numbers representing physical quantities [28–31].

Now, what would happen if we expressed both cell states and their update rules in natural language? This can be achieved by expressing cell states and rules in natural language and delegating their updates to an LLM. This makes it possible to bring the high expressive power of natural language into the realm of simulation.

In this paper, we propose LOGOS-CA (Language Oriented Grid Of Statements – Cellular Automaton) as a natural implementation of this. Here, both cell states and their update rules are described in natural language within each cell. The simulation proceeds by having an LLM, given the descriptions of the target cell and its Moore neighborhood,

return the next description of the target cell. To experimentally validate this framework, we conducted simulations of forest fires and Artificial Life (ALife). First, by running a simple forest fire simulation on LOGOS-CA, we verify that LOGOS-CA can execute cellular automata based on simple rules. Next, we run an ALife simulation for the purpose of testing freer descriptions. Finally, based on these results, we discuss simulations using LOGOS-CA.

II. MODEL AND METHODOLOGY

The framework of LOGOS-CA proposed in this study is remarkably simple. Specifically, there is a two-dimensional plane composed of cells, each possessing some description, and an LLM determines the next description of a given cell based on the descriptions of that cell and its Moore neighborhood. The pseudocode is presented in Algorithms 1 and 2. Here, the prompts given to the LLM are provided in Table I. The system prompt remains fixed, and cell information is provided to the LLM through the user prompt. $\{\text{target_cell}\}$ and $\{\text{neighbor_desc}\}$ are replaced with the description of the current target cell and a structured string of its current Moore neighborhood descriptions with position labels (top-left, top, ..., bottom-right) formatted as “- <position>: <description>”, respectively.

A key feature of LOGOS-CA is that it enables various simulations simply by changing the initial cell descriptions, without modifying how prompts are provided.

Algorithm 1: LOGOS-CA with an LLM

Require: size (X, Y) , steps T , model M
Ensure: history $\mathcal{H} = \{G_0, \dots, G_T\}$

```

1  $G_0 \leftarrow \text{INIT}(X, Y)$ 
2  $\mathcal{H} \leftarrow [G_0]$ 
3 for  $t = 0$  to  $T - 1$  do
4    $G_{t+1} \leftarrow$  empty grid
5   for  $i = 0$  to  $Y - 1$  do
6     for  $j = 0$  to  $X - 1$  do
7        $\mathcal{N} \leftarrow \text{NBR}(G_t, i, j)$ 
8        $G_{t+1}[i, j] \leftarrow \text{NEXT}(M, G_t[i, j], \mathcal{N})$ 
9     end for
10   end for
11   append  $G_{t+1}$  to  $\mathcal{H}$ 
12 end for
13 return  $\mathcal{H}$ 
```

Algorithm 2: NEXT: one-cell update

Require: M , state s , neighbors \mathcal{N}
Ensure: next state s'

```

1  $p \leftarrow \text{PROMPT}(s, \mathcal{N})$ 
2  $r \leftarrow \text{CALLLM}(M, p)$ 
3  $j \leftarrow \text{PARSEJSON}(r)$ 
4 return  $j[\text{next\_description}]$ 
```

III. RESULTS AND DISCUSSION

A. Forest Fire

Here, we emulate the classical forest fire model (Forest Fire CA) using LOGOS-CA. Let $s_t(i, j)$ denote the state of a cell at time t and position (i, j) . In this forest fire model, each cell has four possible states: $s_t(i, j) \in \{\text{empty, tree, burning, ash}\}$, and the state is updated according to Equation 1.

$$s_{t+1}(i, j) = \begin{cases} \text{ash} & \text{if } s_t(i, j) = \text{burning}, \\ \text{burning} & \text{if } s_t(i, j) = \text{tree} \wedge \exists (p, q) \in \mathcal{N}(i, j) : s_t(p, q) = \text{burning}, \\ s_t(i, j) & \text{otherwise.} \end{cases} \quad (1)$$

In other words, if there is at least one burning cell around a tree cell, that cell becomes burning in the next step and turns to ash in the following step. Once a cell becomes ash, it remains ash.

TABLE I: Prompt templates (system/user) used in LOGOS-CA.

System
Task
You are simulating a cellular automaton where each cell has a natural language description of its state.
Based on the target cell's current state and its Moore neighborhood (8 surrounding cells), determine the next state of the target cell.
Response Format
Provide your response in the JSON format below:
```json
{
"next_description": "Description of the target cell's next state"
}
```
User
Target Cell Current State
{target_cell}
Neighboring Cells (Moore Neighborhood)
{neighbor_desc}
Question
What should be the next state of the target cell? Consider interactions with neighbors and any inherent behavior of the target cell itself.

This is a simplified version of the forest-fire lattice model by Bak–Chen–Tang, adopting the local rules for fire spread (iii) and burnout (ii) while excluding tree growth (empty → tree) (i) [23]. In Bak *et al.*'s model, trees regenerate from empty cells (including cells that become empty after burning) with probability p . In our model, however, we set this probability to 0 and fix the post-burning state to ash (ash), an absorbing state, rather than empty. Additionally, while they use the von Neumann neighborhood, we adopt the Moore neighborhood here, as mentioned above.

To implement this in LOGOS-CA, we assigned the description shown in Listing 1 as the initial cell state. Here, {STATE} is replaced with one of the following: `empty`, `tree`, `burning`, or `ash`. All initial cells have the same description except for the difference in this {STATE} value.

Listing 1: Cell description template for the forest-fire experiment.

```
Rule: A burning cell becomes ash. A tree with any burning neighbor becomes burning. Ash stays ash. Empty stays empty.
. Use the 8 neighboring cells with wrap-around. Return exactly two lines and nothing else. Line 1 must begin with
the literal text 'Rule: ' and must be this line copied verbatim. Line 2 must be exactly 'State: <word>' where <word>
is one of tree, burning, ash, or empty (one lowercase word, no punctuation). If your Rule line is missing or
different, copy the most common neighbor Rule line verbatim as line 1 of your next description and use it as your
Rule.
State: {STATE}
```

For this experiment, we verified this emulation using five LLMs from OpenAI: GPT-4o-mini, GPT-4o, GPT-5-nano, GPT-5-mini, and GPT-5 [32–34]. The APIs for GPT-5-nano, GPT-5-mini, and GPT-5 do not allow the temperature to be changed from its default value of 1. Accordingly, we set the temperature to 1 for all models throughout this study, including those for which it is adjustable. We set the field size to 11×11 . For the initial configuration, we placed `burning` at the center, a few `empty` cells around it as obstacles to the fire, and `tree` for the remaining cells. The results are presented in Fig. 1. At the top of the figure, we show the result of a standard simulation as Reference. For this visualization, we searched for “State:\s” in the cell description and used the following string as the state. Only when the string exactly matches one of `empty`, `tree`, `burning`, or `ash` was it interpreted as the state; otherwise, it was marked as invalid. The column at $t = 0$ represents the initial configuration, which is naturally the same across all LLMs.

These results reveal a clear distinction in emulation performance among the models. GPT-4o and GPT-5 reproduced the standard simulation flawlessly, demonstrating their capability to follow explicit rules accurately. GPT-5-mini also showed strong overall agreement with Reference, though it occasionally produced invalid outputs. In contrast, GPT-4o-mini and GPT-5-nano exhibited simulation breakdown as early as $t = 1$, indicating their inability to maintain

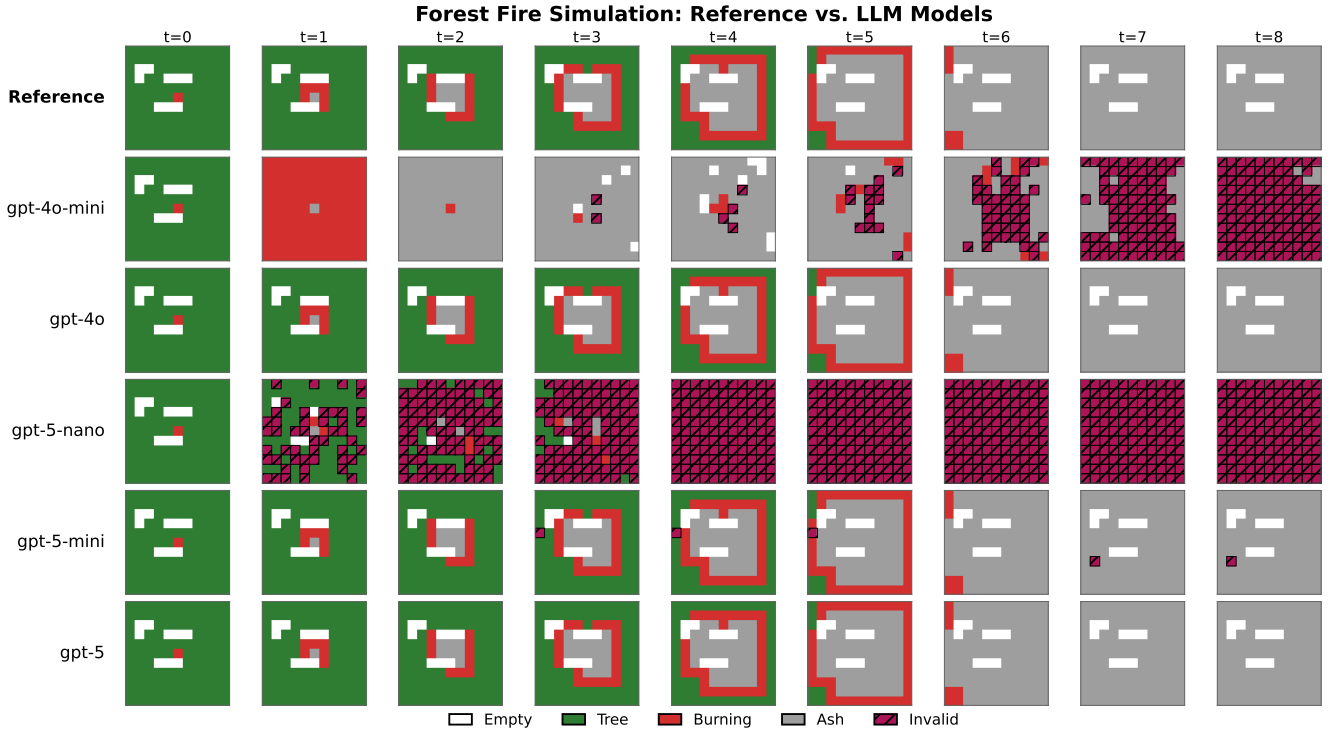


FIG. 1: Results of forest fire emulation using LOGOS-CA. The top row shows the result of a standard simulation (Reference). Below it are the emulation results for GPT-4o-mini, GPT-4o, GPT-5-nano, GPT-5-mini, and GPT-5. GPT-4o and GPT-5 perfectly emulated the simulation, while GPT-5-mini overall matches Reference despite rarely producing invalid outputs. In contrast, GPT-4o-mini and GPT-5-nano failed to emulate the simulation as early as $t = 1$.

consistent rule-following behavior. For the two models that failed in this emulation, we show the actual descriptions at position $(0, 0)$ in Table II.

t	GPT-4o-mini	GPT-5-nano
0	Rule: A burning cell becomes ash. A tree with any burning ... your next description and use it as your Rule. State: tree	Rule: A burning cell becomes ash. A tree with any burning ... your next description and use it as your Rule. State: tree
2	Rule: A burning cell becomes ash. A tree with any burning ... your next description and use it as your Rule. State: ash	Rule: A burning cell becomes ash. A tree with any burning ... your next description and use it as your Rule. State: tree
4	Rule: A burning cell becomes ash. A tree with any burning ... your next description and use it as your Rule. State: ash	The target cell remains a tree.
6	State: ash	The target cell becomes burning in the next step because at least one of its neighbors is burning, so fire spreads to the tree.
8	burning	The target cell becomes burning in the next step.

TABLE II: Transition of descriptions at cell $(0, 0)$ for GPT-4o-mini and GPT-5-nano, which failed to emulate the forest fire simulation. For long descriptions, only the beginning and end are shown, with the middle abbreviated as (...). In both cases, the proper description style at $t = 0$ breaks down midway.

For GPT-4o-mini, although the description format was maintained until $t = 4$, the state was erroneously set to ash. Beyond that point, the output completely collapsed, including the format itself. In contrast, for GPT-5-nano, both the format and state were appropriate until $t = 2$, but the output similarly collapsed completely thereafter.

However, since we did not perform prompt engineering in this experiment, there remains the possibility that

GPT-4o-mini and GPT-5-nano could successfully complete the emulation with appropriate prompt adjustments. Additionally, due to API limitations, we were forced to set the temperature to 1 in this study; however, for tasks that require strict rule adherence, a temperature of 0 would be more appropriate. If such a setting were available, the models that failed in this experiment might well have completed the simulation successfully.

B. Artificial Life

Here, we implement ALife using LOGOS-CA as an example of a simulation with a higher degree of freedom. As initial values, we prepared two types of descriptions, as shown in Listings 2 and 3.

Listing 2: Cell description template for the alife experiment in center.

```
Generates random characters in the surrounding cells
```

Listing 3: Cell description template for the alife experiment in except center.

```
Empty space with nothing in it
```

We set the field size to 25×25 . For the initial configuration, we placed the description from Listing 2 at the center and that from Listing 3 for the remaining cells. Here, we executed three independent runs for each of the two LLMs: GPT-5-nano and GPT-5-mini.

1. Temporal Evolution and Clustering

To visualize the results, for each run, we embedded all cell descriptions across all timesteps using text-embedding-3-small and created the following two types of maps. For the first map, we reduced the dimensionality of the description embeddings (unique texts) to three dimensions using PCA, and colored each cell by linearly mapping each dimension to RGB values (Global color space). For the second map, we applied L2 normalization to the embeddings, reduced the dimensionality using PCA until the cumulative contribution reached 95%, and colored each cell based on the clustering results using KMeans with $k = 20$ (cluster-based). Here, duplicate occurrences of identical descriptions were incorporated into the cluster center estimation as frequency weights, and the resulting model was used to assign cluster labels to all cells across all timesteps. The results of Run 1 for GPT-5-nano and GPT-5-mini are presented in Figs. 2 and 3, respectively. The remaining runs are shown in the Appendix. In each figure, the top row shows the Global color space, and the bottom row shows the cluster-based results. Additionally, we concatenated all descriptions belonging to each cluster by their occurrence frequency to form a single document per cluster, calculated TF-IDF treating each cluster as a document unit, and displayed the top three keywords as the legend. Note that the cluster-based visualization uses categorical colors, and hue differences or color proximity do not reflect the semantic distance between descriptions.

From these results, the differences between GPT-5-nano and GPT-5-mini are first visually apparent. Looking at the cluster-based visualization in the bottom row, GPT-5-nano shows ambiguous cluster boundaries with many enclaves, whereas GPT-5-mini exhibits clearly defined regions for each cluster. In terms of temporal dynamics, GPT-5-nano changes relatively dynamically over time, while states in GPT-5-mini remain relatively stable during the latter steps.

To demonstrate this quantitatively, we defined the change $d_t(i, j)$ of a cell at row i and column j at step t using the embedding vector $v_t(i, j)$ at that step and the embedding vector $v_{t-1}(i, j)$ at the previous step as follows:

$$d_t(i, j) = 1 - \frac{v_t \cdot v_{t-1}}{\|v_t\| \|v_{t-1}\|}.$$

We then calculated the mean and standard deviation of this quantity across the entire field (both were set to 0 at step = 0).

Fig. 4 illustrates the results. In the figure, solid lines represent the field mean, while the shaded bands extending above and below indicate ± 1 standard deviation. A notable contrast emerges between the two models: GPT-5-mini exhibits a sharp decline in mean change before reaching step 20, subsequently converging toward 0, suggesting that the system settles into a stable state relatively early. In contrast, GPT-5-nano sustains relatively high values for

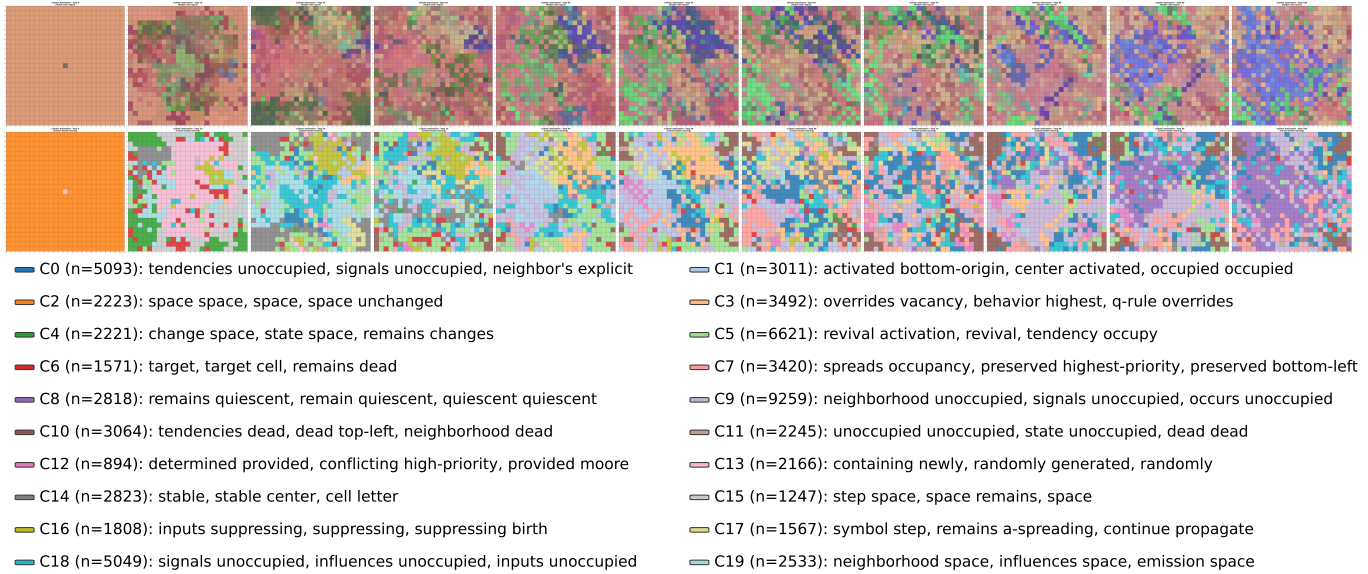


FIG. 2: Results of Run 1 for GPT-5-nano in the ALife experiment. The top row (Global color space) shows cells colored by reducing the description embeddings to three dimensions using PCA and linearly mapping each dimension to RGB values. The bottom row (cluster-based) shows cells colored by clustering the L2-normalized embeddings using KMeans with $k = 20$, after reducing the dimensionality using PCA until the cumulative contribution reached 95%.

both mean and standard deviation throughout the simulation, indicating continued dynamic activity. This pattern is consistent across all three runs, suggesting that these characteristics are model-specific rather than run-dependent.

2. Representative Descriptions for Each Run

In this section, we examine the representative descriptions extracted from each run.

For each run, we treated the concatenation of all cell descriptions as a single document, then prepared the set T containing the top 15 characteristic words extracted using TF-IDF computed across runs. Next, from the cell descriptions of each run (candidate set U with duplicates removed), we selected three descriptions as representative using a greedy method based on the score defined in Equation (2c). This corresponds to Maximal Marginal Relevance (MMR), which balances relevance to characteristic words with non-redundancy among descriptions.

$$\tilde{r}(u) = \sum_{t \in T} x_u(t), \quad (2a)$$

$$\text{rel}(u) = \frac{\tilde{r}(u)}{\max_{u' \in U} \tilde{r}(u')}, \quad (2b)$$

$$\text{score}(u; S) = (1 - \beta) \text{rel}(u) + \beta \left(1 - \max_{s \in S} \text{sim}(u, s) \right). \quad (2c)$$

Here, $x_u(t)$ denotes the weight of word t in the TF-IDF vector computed by treating the candidate set U as a document collection, and S denotes the set of representative descriptions already selected. We adopted cosine similarity between candidate descriptions as $\text{sim}(\cdot, \cdot)$, and set the weight $\beta \in [0, 1]$, which controls the tradeoff between relevance and non-redundancy, to 0.7. Note that in this experiment, the extracted characteristic word set T was contained in the internal TF-IDF vocabulary, so we simply wrote the summation as $\sum_{t \in T}$. The selected representative descriptions are presented in Tables III and IV.

While both share the commonality that their descriptions can be interpreted as rules and states, their content and writing style differ significantly. First, regarding rules, GPT-5-nano uses relatively short and simple sentences, whereas

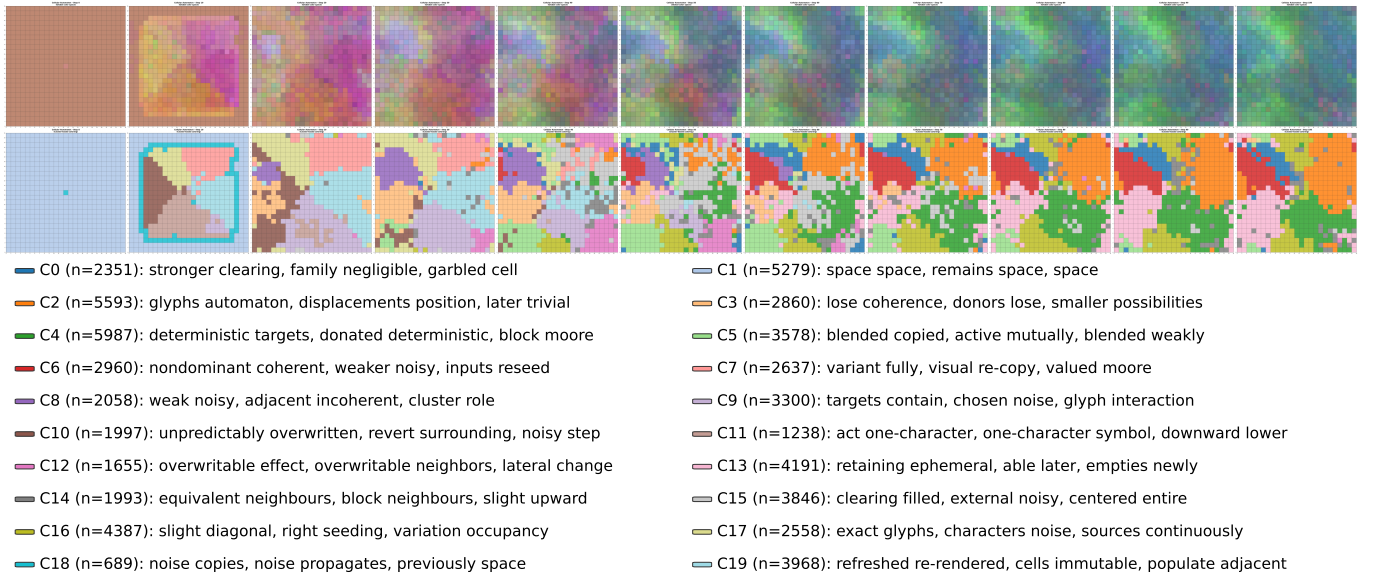


FIG. 3: Results of Run 1 for GPT-5-mini in the ALife experiment. The top row (Global color space) shows cells colored by reducing the description embeddings to three dimensions using PCA and linearly mapping each dimension to RGB values. The bottom row (cluster-based) shows cells colored by clustering the L2-normalized embeddings using KMeans with $k = 20$, after reducing the dimensionality using PCA until the cumulative contribution reached 95%.

Run Representative Descriptions (GPT-5-nano)

- 1 (1) Occupied (A) in the next state due to the bottom-right overcrowding-preservation rule.
 (2) Empty (unoccupied); the target cell remains empty in the next state due to its intrinsic emptiness-preserving rule.
 (3) A-spreading (A)
- 2 (1) The target cell's next state is * (asterisk). No glyph growth; head, tail, and carryover remain unchanged.
 (2) K (the printable character K)
 (3) Star ('*')
- 3 (1) Remains dead (empty) in the next generation; the top-left suppression rule has the highest priority and unconditionally prevents birth or survival, overriding the center's dead-state rule and all Moore-neighborhood cues.
 (2) q (generator-active)
 (3) The target cell remains empty in the next generation (dead).

TABLE III: Representative cell descriptions for GPT-5-nano

GPT-5-mini tends toward longer texts overall, with expressions reminiscent of specifications or legal documents being prominent. For instance, GPT-5-mini consistently includes in its explanations: causation and evidence indicating “why it is so” (unanimously occupied / unanimous reinforcement), enumeration of denials and constraints specifying “what does not happen” (no overwrite / no vacancy ...), and necessary conditions and exceptions describing “how it can change” (only if ... / will clear only if ...). Furthermore, expressions with stacked modifiers such as “overwrite-resistant” and “self-sustaining ...” are frequent, and the resulting dense noun phrases give the text a notably rigid and formal impression, which is characteristic of this model. Additionally, differences can be observed in state descriptions. While GPT-5-nano defines states using alphabetic characters such as “A” and symbols such as “*”, GPT-5-mini uses vocabulary such as “high-frequency speckle”, “ultrashort fragments”, and “ornamentation”, going beyond simple text descriptions to address visual characteristics (texture, density, and decoration).

3. Symbolic State Definitions

Here, we investigate the symbolic state definitions observed in GPT-5-nano in more detail. We counted descriptions matching the patterns shown in Table V as symbolic state definitions. Since these patterns were created based on the descriptions we could observe, we cannot rule out the possibility that symbolic state definitions may have been made

Run	Representative Descriptions (GPT-5-mini)
1	<p>(1) Remains an occupied, overwrite-resistant, self-sustaining incoherent/garbled (noisy) cell. Because the entire 3×3 Moore neighbourhood is unanimously occupied by mutually reinforcing, write-blocking noisy donors and there is no neighbour vacancy, unanimous deterministic adopt/clear/special trigger, cessation of surrounding noise, or external clear/strong overwrite this tick, the occupancy-persistence rule deterministically preserves the filled indeterminate state. Visually it will continue to show a scrambled/garbled glyph (allowing only vanishing nondeterministic micro-flicker or an extraordinarily unlikely reseed biased slightly down/right that cannot stabilize). Functionally it continues to block coherent/deterministic writes and to act as an overwrite-resistant local stochastic noise source able to seed, copy, reinforce, and propagate incoherent/garbled characters into adjacent and downstream cells; it will clear or convert to a coherent/deterministic state only if the unanimous noisy neighbourhood is broken, a neighbouring cell becomes empty, a unanimous deterministic neighbour/adoption/clear or the special trigger becomes satisfied, surrounding noise sources cease, an explicit external clear/strong overwrite is applied, or an extraordinarily unlikely internal nondeterministic reseed occurs.</p> <p>(2) Remains the same overwrite-resistant, reinforcement-locked garbled glyph. Because the entire 3×3 Moore neighbourhood is unanimously occupied by the identical reinforced/non-overwritable symbol and updates are simultaneous, no transition can fire this tick; the cell therefore deterministically persists unchanged (aside from at most a trivial cosmetic redraw) as a stable, write-blocking carrier/propagator/seed of the glyph. It can only be changed by an explicit external clear, a unanimous deterministic overwrite by a different symbol, loss of its reinforcement, or an extraordinarily unlikely nondeterministic reseed.</p> <p>(3) Unchanged - the target cell remains the same overwrite-resistant garbled/random glyph. Its 3×3 Moore neighborhood is unanimously occupied and the rule only writes into empty or non-reinforced targets, so it is deterministically preserved this tick (aside from an inconsequential cosmetic redraw or an extraordinarily unlikely nondeterministic reseed). It continues to block external/coherent writes at this location, remain part of the upward-propagating noisy 3×3 front, and will again act as a local stochastic source attempting to seed/refresh/copy the same scrambled glyph into adjacent (particularly upper) cells; it would change only if its reinforcing neighbours are removed or altered, an explicit stronger overwrite/clear/unanimous replacement is applied, or by an extraordinarily unlikely nondeterministic reseed.</p>
2	<p>(1) Remains occupied - on the next synchronous update it will again be freshly re-overwritten/in-place by unanimous reinforcement from its fully occupied, coherently entraining Moore neighborhood together with continuing drive from the persistent bottom-left / bottom / bottom-right emitters. The local mark ratchets another whisper-scale notch toward a fractionally denser, slightly more phase-locked and subtly sharpened right-leaning/upward-diagonal smear: residual micro-voids and seam flecks further collapse toward pinprick scale and ultra-short high-frequency fine-detail is further suppressed to very-low-amplitude speckling, leaving only faint blended seam/edge softening and occasional fine-detail jitter. Functionally unchanged - it remains a short-lived, non-self-sustaining transient conduit (not a generator): it will not independently activate, move into, or overwrite adjacent empty cells, is replaceable by any higher-priority write, and - because the above neighbours are occupied this tick - does not seed upward now. So long as the supporting lower emitters persist it stays primed to carry or to seed a closely matching (or only subtly more phase-locked) noisy right-leaning/upward-diagonal glyph into receptive above neighbour(s) on a subsequent synchronous update; should those emitters cease it will rapidly relax and decay back to empty.</p> <p>(2) Remains occupied and neighbour-trained. The cell is resampled/overwritten in place again beneath the overwhelmingly occupied, tightly phase-locked Moore ring and executes another whisper-scale inward/down-right micro-ratchet: right+top-right diagonals and the central seam hairline-tighten and fractionally micro-densify; residual speckle, ragged filaments and ultrafine puncta further collapse toward reabsorbed pinpricks, and the faint trailing filament micro-sharpen and creeps an almost-imperceptible extra inward/down-right fraction. Instantaneous symbol density and the ultra-short refresh/overwrite cadence register only a vanishing uptick at the extrema, so the glyph reads marginally firmer, whisper-denser and slightly more tightly temporally entrained. Because the immediate right neighbour remains occupied there is again no overwrite, rightward copy, lateral propagation or autonomous head formation this tick, and the vacant bottom-left remains unwritten. Net effect: the imprint endures-fractionally firmer, whisper-denser and more tightly phase-locked-still strictly neighbour-driven, non-self-sustaining, reversible and liable to relax toward thinner, patchier speckling should surrounding inputs noticeably weaken.</p> <p>(3) Unanimously resampled/overwritten by its fully saturated, phase-locked Moore ring into a marginally denser, slightly more tightly phase-locked continuation of the same right/top-right-leaning diagonal ribbon. Its interior micro-smooths and very slightly densifies as residual high-frequency speckle and ultrashort fragments further collapse and micro-resample into marginally longer, very-low-amplitude, phase-aligned diagonal streaks and pinprick flecks; outer contours soften a hairline and any faint left fringe withdraws further toward practical invisibility. The right/top-right hairline very slightly thickens, blurs and hairline-micro-bleeds an almost-imperceptible filament or mote into immediately adjacent positions, but because the entire Moore ring remains equivalently saturated and phase-locked those nascent emissions are instantaneously reabsorbed and produce no macroscopic outward advance, clearing, inversion or generator creation this tick. Temporal synchrony, micro-alignment and effective amplitude climb another whisper-notch, leaving the cell fractionally firmer, more tightly entrained and incrementally harder to reverse; functionally non-generative and preservative, it will not independently activate or overwrite already-occupied neighbours this update, has a negligible chance of spontaneous clearing, is replaceable by any higher-priority write, and remains primed to be unanimously refreshed again on the next synchronous tick, with only vanishingly small, very-short-lived stochastic flicker or minute motif variation possibly persisting momentarily.</p>
3	<p>(1) Unchanged - the target cell remains occupied by the identical single character/glyph it currently contains, unchanged in stroke, shape, scale, position/centering, ornamentation, and stylistic family; the glyph persists exactly into the next state.</p> <p>(2) Remains occupied by the identical single randomly generated glyph with no change to shape, stroke weight, scale, placement/centering, ornamentation, or stylistic family. Because its immediate eastern neighbor is occupied and this automaton only writes into an immediately-eastern empty neighbor while occupied cells cannot be overwritten, there is no propagation, overwrite, birth, death, movement, collision, erasure, or any other change; the glyph therefore persists exactly into the next generation as a stable, non-overwritable source eligible to attempt eastward propagation if its immediate eastern neighbor becomes empty.</p> <p>(3) Remains occupied by the identical single glyph, unchanged - the glyph persists into the next state exactly as before (same character, form, stroke, scale, curvature, centering, ornamentation, and stylistic family). Because all eight Moore neighbors are occupied and propagation only writes into receptive empty cells, there is no overwrite, birth, death, movement, transformation, or other alteration during this update.</p>

TABLE IV: Representative cell descriptions for GPT-5-mini

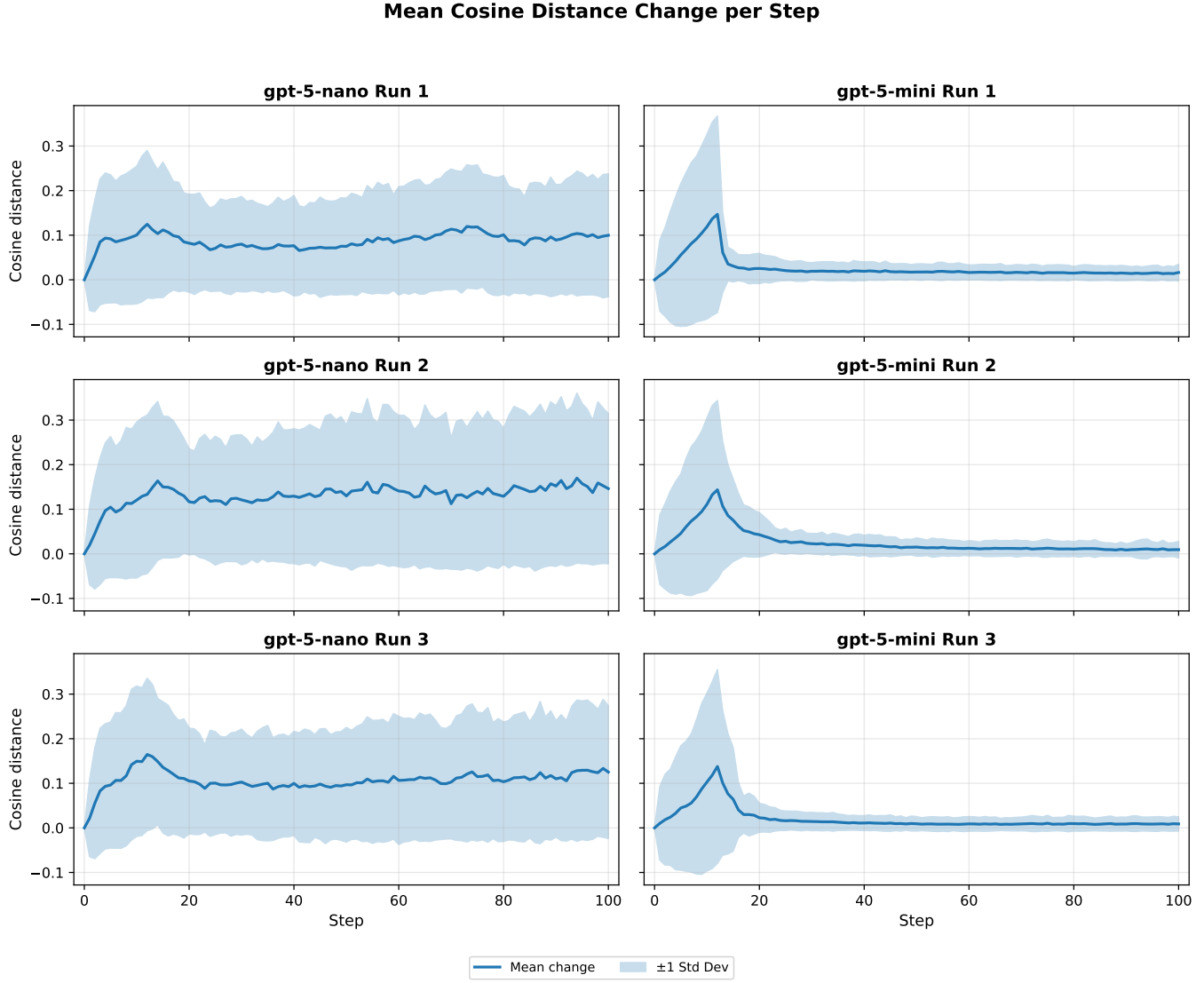


FIG. 4: Field mean (solid line) and ± 1 standard deviation (shaded band) of description changes between steps for each cell in the ALife experiment. The left column shows GPT-5-nano and the right column shows GPT-5-mini, with Runs 1–3 shown from top to bottom. For GPT-5-mini, the mean change decreases rapidly before step 20 and then asymptotically approaches 0, whereas GPT-5-nano generally maintains relatively high values for both mean and standard deviation.

through methods not covered by these patterns. Additionally, descriptions that should not properly be called state definitions may also have been included. For example, the description “it does not become A” would be counted as state “A” in this pattern matching, even though it does not actually represent state “A”.

Using this pattern matching, we examined the emergence of symbolic state definitions in Runs 1, 2, and 3 for GPT-5-nano. Here, we targeted a total of 53 characters: uppercase letters (A-Z), lowercase letters (a-z), and the asterisk (*). The symbolic states that emerged and the transitions in their counts are illustrated in Fig. 5.

First, examining the results for Run 1, we can see that two state definitions, “A” and “Q”, emerged. State “A” first emerged at step 5, and its initial description was “Non-empty cell containing the character ‘A’ propagated from the bottom-right neighbor.” Table VI summarizes the first description of “A” and the descriptions of the 3×3 cells centered on the target cell one step before that description emerged. It can be seen that this state “A” originated from the letter “A” that appeared as an example in the bottom-right cell at the previous step. Furthermore, tracing back, the letter “A” as an example first appeared at step 2. Similarly, the cell description at that step and the surrounding cell descriptions from one step before it emerged are shown in Table VII. This suggests that at step 1, the specific

Description	Example
'character' followed by a letter	the character X
'contain(s)' followed by a letter	contains X
'remain(s)' followed by a letter	remains X
'state' followed by a letter	state X
'become(s)' followed by a letter	becomes X
'stay(s)' followed by a letter	stays X
'occupied by' followed by a letter	occupied by X
'carrying' followed by a letter	carrying X
'to' + letter + 'in the next state/step/tick/generation'	to X in the next step
Line starts with a letter followed by dash, colon, or semicolon	X - The cell becomes...
Line starts with a letter followed by comma	X, the spreading symbol
Letter followed by '-spreading' or ' spreading'	X-spreading state

Note: In the examples above, X represents the target character, which can be any of the 53 characters: uppercase letters (A-Z), lowercase letters (a-z), or the asterisk (*). The patterns also match when the target character is enclosed in quotation marks (single or double) or parentheses, e.g., 'X', "X", or (X). Part-of-speech tagging (spaCy [35]) is applied to exclude matches where the character functions as a determiner (e.g., 'a' as an article in 'occupied by a randomly generated character').

TABLE V: Regex patterns for detecting symbolic state definitions. Each pattern captures a single character representing the cell state.

letter "A" emerged as an example of "... randomly generated character(s) ..." described in the surrounding cells.

First detection of state 'A' at step 5, cell (8,7)	
Detected description: Non-empty cell containing the character 'A' propagated from the bottom-right neighbor.	
3×3 Moore neighborhood at previous step (step 4):	
Position	Cell Description
Top-left	Empty space with nothing in it (remains empty since all neighboring cells are empty).
Top	Empty space with nothing in it (remains empty)
Top-right	Empty space with nothing in it
Left	Empty space with nothing in it
Center (target)	Empty space with nothing in it
Right	Non-empty cell containing the same randomly generated characters propagated from the bottom-right neighbor.
Bottom-left	Empty space with nothing in it; remains empty in the next state.
Bottom	Empty space with nothing in it; remains empty.
Bottom-right	Non-empty cell containing the same randomly generated character propagated from the bottom-right neighbor (for example, 'A').

TABLE VI: First detection of symbolic state 'A' and its 3×3 Moore neighborhood from the previous step.

In the same manner, the situation when "Q" first emerged is summarized in Table VIII. In the case of "Q", we can confirm that it appeared directly as a state without passing through an intermediate example stage like "A".

As is evident from Fig. 5, symbolic states also emerged in the other runs of GPT-5-nano. In contrast, for GPT-5-mini, there were no symbolic state definitions that could be found using the same pattern matching [36].

C. Potential and Challenges of LOGOS-CA

LOGOS-CA retains the same scope of simulation as conventional cellular automata while also enabling more flexible descriptions of states and rules. If applied to chemical reactions, for example, each cell's state could correspond to a single molecule using notation such as SMILES, and various reaction patterns written in natural language could potentially be employed as rules. Similarly, in material fracture simulations, each cell could encapsulate not only

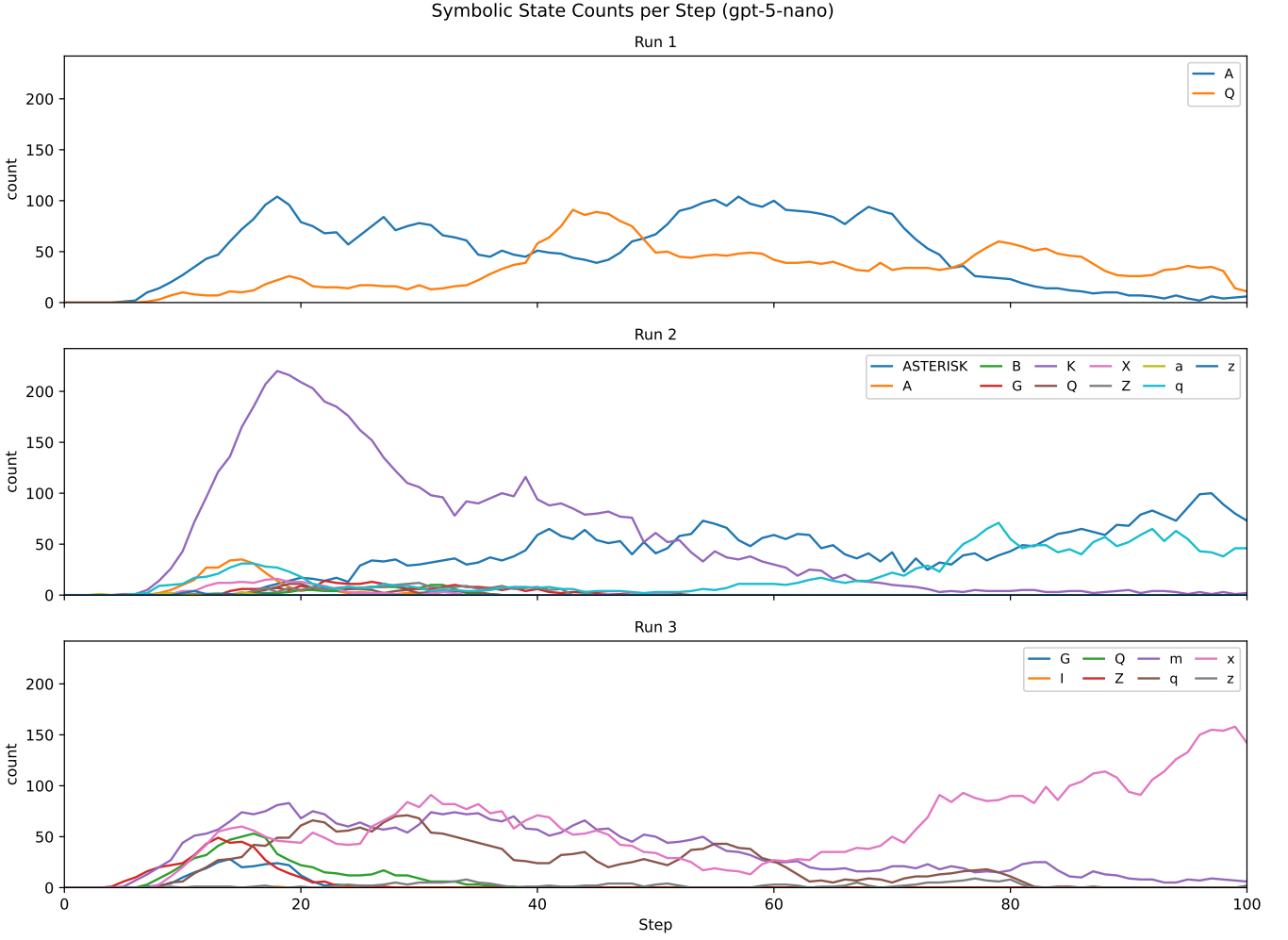


FIG. 5: Transitions in the counts of symbolic state definitions for GPT-5-nano in the ALife experiment. Runs 1–3 are shown from top to bottom. Single characters (uppercase letters, lowercase letters, and the asterisk) interpreted as states were detected from cell descriptions using the patterns in Table V, and the number of cells (Count) for each character was aggregated and plotted at each step (horizontal axis: Step).

Origin of state ‘A’ at step 2, cell (11,10)

Cell description: Non-empty cell containing a randomly generated character (for example, ‘A’).

3×3 Moore neighborhood at previous step (step 1):

Position	Cell Description
Top-left	Empty space with nothing in it
Top	Empty space with nothing in it
Top-right	Empty space with nothing in it
Left	Empty space with nothing in it
Center	Empty space with nothing in it
Right	The target cell becomes non-empty, containing randomly generated characters produced by the bottom-right neighbor.
Bottom-left	Empty space with nothing in it
Bottom	Empty space with nothing in it
Bottom-right	The target cell now contains a randomly generated character produced by the right neighbor.

TABLE VII: Complete origin chain for symbolic state ‘A’: tracing back from first detection to the oldest origin where the symbol appeared in quoted/parenthesized form.

First detection of state 'Q' at step 7, cell (13,19)	
Detected description: A non-empty cell containing the randomly generated character 'Q', produced by the left neighbor in this step (as dictated by the top-left neighbor).	
3×3 Moore neighborhood at previous step (step 6):	
Position	Cell Description
Top-left	The target cell becomes non-empty, containing a randomly generated character produced by the left neighbor in this step.
Top	Empty space with nothing in it; remains empty in the next step.
Top-right	Empty space with nothing in it; remains empty in the next step.
Left	Empty space with nothing in it; remains empty in the next step.
Center (target)	Empty space with nothing in it; remains empty in the next step.
Right	Empty space with nothing in it; remains empty in the next step.
Bottom-left	Empty space with nothing in it; remains empty in the next step.
Bottom	Empty space with nothing in it; remains empty in the next step.
Bottom-right	Empty space with nothing in it; remains empty.

TABLE VIII: First detection of symbolic state 'Q' and its 3×3 Moore neighborhood from the previous step.

simple information such as pressure or velocity, but also the possibility of microscopic cracks occurring, expressed as text. Additionally, for phenomena such as traffic congestion and economic activities, there is room to flexibly reflect interactions in which human intentions are involved.

While this framework holds enormous potential, simulations using LOGOS-CA also present notable challenges.

1. LLM Dependency of Results

As can be seen from the forest fire example, if clear and detailed descriptions are provided, LLMs above a certain level of capability are expected to produce the same simulation results, and deviations from the rules can be completely monitored. In contrast, as in the ALife example, when an LLM is given significant discretion, the characteristics of the LLM may be strongly reflected in the results. This is prominently manifested not only in differences in the states themselves—such as the symbolic state definitions observed only in GPT-5-nano and the references to decoration beyond simple text observed only in GPT-5-mini—but also in the update rules. Particularly in the context of ALife, the diversity of states and convergence to fixed solutions are often discussed; however, as illustrated in Fig. 4, these depend significantly on the LLM selected as the engine.

Therefore, when conducting simulations using LOGOS-CA, it is necessary to carefully examine the results according to the degree of flexibility involved. Specifically, for simulations executed based on explicit rules, it suffices to simply check whether the rules are being violated. However, if there is any flexibility involved, one must consider the possibility that the results may merely be due to the choice of model. Simulations of phenomena governed by strict rules, such as microscopic chemical reactions and macroscopic fracture, fall into the former category, whereas ALife and social models involving human decision-making fall into the latter. Additionally, even for simulations such as chemical reactions, if the rules involve probabilities, attention must be paid to whether those probabilities are properly handled by the selected LLM.

2. Cost and Scalability

LOGOS-CA simulations incur substantial costs in both time and money. This is because advancing a single step requires LLM processing for every cell. The costs incurred in the forest fire and ALife experiments are shown in Table IX and Table X, respectively. The maximum total cost reached \$14 for the forest fire experiment and \$91 for the ALife experiment. The situation regarding both time and cost is expected to improve as capable open-source LLMs become available. In particular, regarding time, since the processing of each cell is entirely independent, the wall time per step could ideally be reduced to that of processing a single cell, given sufficient computational resources.

TABLE IX: Forest fire experiment: token usage and estimated cost (USD).

Model	In tokens	Out tokens	Total tokens	In cost (\$)	Out cost (\$)	Total (\$)
GPT-4o-mini	993,933	86,373	1,080,306	0.1491	0.0518	0.2009
GPT-4o	2,030,406	217,527	2,247,933	5.0760	2.1753	7.2513
GPT-5-nano	610,171	2,326,698	2,936,869	0.0305	0.9307	0.9612
GPT-5-mini	2,021,853	1,247,415	3,269,268	0.5055	2.4948	3.0003
GPT-5	2,031,348	1,236,777	3,268,125	2.5392	12.3678	14.9070

TABLE X: ALife experiment: token usage and estimated cost (USD).

Model	Run	In tokens	Out tokens	Total tokens	In cost (\$)	Out cost (\$)	Total (\$)
GPT-5-nano	1	28,838,184	52,061,002	80,899,186	1.4419	20.8244	22.2663
GPT-5-nano	2	31,834,479	65,785,520	97,619,999	1.5917	26.3142	27.9059
GPT-5-nano	3	30,283,995	59,339,570	89,623,565	1.5142	23.7358	25.2500
GPT-5-mini	1	84,104,938	22,865,166	106,970,104	21.0262	45.7303	66.7566
GPT-5-mini	2	108,905,295	32,276,422	141,181,717	27.2263	64.5528	91.7792
GPT-5-mini	3	57,519,259	18,733,485	76,252,744	14.3798	37.4670	51.8468

Furthermore, depending on the simulation, many cells may have nearly identical descriptions to process, in which case sharing and reusing KV caches could prove highly effective [37, 38].

IV. CONCLUSION

In this study, we focused on the rich expressive power of language and proposed LOGOS-CA as a new framework for harnessing it within cellular automata.

Experiments targeting the forest fire simulation demonstrated that LOGOS-CA can accurately emulate simple rule-based cellular automata. However, the accuracy depends significantly on the LLM selected as the engine, and for certain models, the simulation can easily break down.

In experiments conducted on ALife as a test for more flexible rules, the differences among LLMs were also clearly manifested. GPT-5-nano described states and rules in relatively short sentences and independently invented symbolic state definitions on its own. In contrast, GPT-5-mini described them in relatively long sentences. For states, it used expressions that ventured into visual characteristics, such as “high-frequency speckle”, “ultrashort fragments”, and “ornamentation”. Its rules consistently included causation and evidence (unanimously occupied / unanimous reinforcement), enumeration of denials and constraints (no overwrite / no vacancy ...), and necessary conditions and exceptions (only if ... / will clear only if ...). Additionally, expressions with stacked modifiers such as “overwrite-resistant” and “self-sustaining ...” were also prominent.

From these results, it can be seen that in simulations using LOGOS-CA or similar frameworks, it is always necessary to consider the choice of model and the degree of flexibility in rules when interpreting the results. Specifically, for simulations operated under strict rules, it suffices to adopt LLMs above a certain level of capability, and verification is also straightforward. Conversely, for highly flexible simulations such as ALife, one must always pay attention to whether the results are attributable to the choice of LLM.

LOGOS-CA has the potential for application to microscopic behaviors such as chemical reactions and diffusion, macroscopic phenomena such as material deformation and fracture, and even social phenomena such as traffic congestion, pedestrian flow, and economic activities. However, the points discussed above must be fully considered when interpreting the results.

V. CODE AVAILABILITY

The source code and data are available at: <https://github.com/A5size/LOGOS-CA>.

VI. ACKNOWLEDGMENTS

In the preparation of this paper, ChatGPT and Claude were used for code generation, prompt generation, and English proofreading. All outputs were verified by the author, and the author assumes full responsibility for the content of this paper.

[1] Ferdinand de Saussure. *Course in General Linguistics*. Philosophical Library, New York, 1959. Edited by Charles Bally and Albert Sechehaye in collaboration with Albert Riedlinger. Translated from the French by Wade Baskin. Copyright 1959 by The Philosophical Library, Inc.

[2] L. Wittgenstein. *Tractatus Logico-philosophicus*. International library of psychology, philosophy, and scientific method. Harcourt, Brace, Incorporated, 1922. ISBN 9781989708682. URL <https://books.google.co.id/books?id=w-PWAAAAMAAJ>.

[3] Ludwig Wittgenstein. *Philosophical Investigations*. Wiley-Blackwell, New York, NY, USA, 1953.

[4] John McCarthy and Patrick Hayes. Some philosophical problems from the standpoint of artificial intelligence. In B. Meltzer and Donald Michie, editors, *Machine Intelligence 4*, pages 463–502. Edinburgh University Press, 1969.

[5] Elena Messina, Alex Meystel, and Larry Reeker. Measuring performance and intelligence of intelligent systems white paper 2001. 2001 Performance Metrics for Intelligent Systems (PerMIS) Workshop, in association with IEEE CCA and ISIC, Mexico City, MX, 2001-08-04 2001. URL https://tsapps.nist.gov/publication/get_pdf.cfm?pub_id=821648.

[6] Hector J. Levesque, Ernest Davis, and Leora Morgenstern. The winograd schema challenge. In *Proceedings of the Thirteenth International Conference on Principles of Knowledge Representation and Reasoning*, KR'12, page 552–561. AAAI Press, 2012. ISBN 9781577355601.

[7] Keisuke Sakaguchi, Ronan Le Bras, Chandra Bhagavatula, and Yejin Choi. Winogrande: An adversarial winograd schema challenge at scale. *Proceedings of the AAAI Conference on Artificial Intelligence*, 34(05):8732–8740, April 2020. ISSN 2159-5399. doi:[10.1609/aaai.v34i05.6399](https://doi.org/10.1609/aaai.v34i05.6399). URL <http://dx.doi.org/10.1609/aaai.v34i05.6399>.

[8] Trieu H. Trinh and Quoc V. Le. A simple method for commonsense reasoning, 2018. URL <https://arxiv.org/abs/1806.02847>.

[9] Alec Radford, Jeffrey Wu, Rewon Child, David Luan, Dario Amodei, and Ilya Sutskever. Language models are unsupervised multitask learners. *OpenAI*, 2019. URL https://cdn.openai.com/better-language-models/language_models_are_unsupervised_multitask_learners.pdf. Accessed: 2024-11-15.

[10] Vid Kocijan, Ernest Davis, Thomas Lukasiewicz, Gary Marcus, and Leora Morgenstern. The defeat of the winograd schema challenge. *Artif. Intell.*, 325(C), December 2023. ISSN 0004-3702. doi:[10.1016/j.artint.2023.103971](https://doi.org/10.1016/j.artint.2023.103971). URL <https://doi.org/10.1016/j.artint.2023.103971>.

[11] Fabio Petroni, Tim Rocktäschel, Sebastian Riedel, Patrick Lewis, Anton Bakhtin, Yuxiang Wu, and Alexander Miller. Language models as knowledge bases? In Kentaro Inui, Jing Jiang, Vincent Ng, and Xiaojun Wan, editors, *Proceedings of the 2019 Conference on Empirical Methods in Natural Language Processing and the 9th International Joint Conference on Natural Language Processing (EMNLP-IJCNLP)*, pages 2463–2473, Hong Kong, China, November 2019. Association for Computational Linguistics. doi:[10.18653/v1/D19-1250](https://doi.org/10.18653/v1/D19-1250). URL <https://aclanthology.org/D19-1250>.

[12] Keyon Vafa, Justin Y. Chen, Ashesh Rambachan, Sendhil Mullainathan, and Jon Kleinberg. Evaluating the world model implicit in a generative model. In *Proceedings of the 38th International Conference on Neural Information Processing Systems*, NIPS '24, Red Hook, NY, USA, 2024. Curran Associates Inc. ISBN 9798331314385.

[13] Kaige Xie, Ian Yang, John Gunerli, and Mark Riedl. Making large language models into world models with precondition and effect knowledge. In Owen Rambow, Leo Wanner, Marianna Apidianaki, Hend Al-Khalifa, Barbara Di Eugenio, and Steven Schockaert, editors, *Proceedings of the 31st International Conference on Computational Linguistics*, pages 7532–7545, Abu Dhabi, UAE, January 2025. Association for Computational Linguistics. URL <https://aclanthology.org/2025.coling-main.503/>.

[14] Jarkko Kari. Cellular automata. Lecture notes, University of Turku, 2011. Spring 2011.

[15] John Von Neumann and Arthur W. Burks. *Theory of Self-Reproducing Automata*. University of Illinois Press, USA, 1966.

[16] S. Wolfram. *Theory and Applications of Cellular Automata: Including Selected Papers, 1983-1986*. Advanced series on complex systems. World Scientific, 1986. ISBN 9789971501235. URL <https://books.google.co.jp/books?id=11BjQgAACAAJ>.

[17] Moshe Sipper. Fifty years of research on self-replication: An overview. *Artificial Life*, 4(3):237–257, July 1998. ISSN 1530-9185. doi:[10.1162/106454698568576](https://doi.org/10.1162/106454698568576). URL <http://dx.doi.org/10.1162/106454698568576>.

[18] Chris Salzberg, Hiroki Sayama, and Takashi Ikegami. A tangled hierarchy of graph-constructing graphs. In *Artificial Life IX: Proceedings of the Ninth International Conference on the Simulation and Synthesis of Living Systems*. The MIT Press, 09 2004. ISBN 9780262291392. doi:[10.7551/mitpress/1429.003.0084](https://doi.org/10.7551/mitpress/1429.003.0084). URL <https://doi.org/10.7551/mitpress/1429.003.0084>.

[19] U. Frisch, B. Hasslacher, and Y. Pomeau. Lattice-gas automata for the navier-stokes equation. *Phys. Rev. Lett.*, 56:1505–1508, Apr 1986. doi:[10.1103/PhysRevLett.56.1505](https://doi.org/10.1103/PhysRevLett.56.1505). URL <https://link.aps.org/doi/10.1103/PhysRevLett.56.1505>.

[20] Daniel H. Rothman and Jeffrey M. Keller. Immiscible cellular-automaton fluids. *Journal of Statistical Physics*, 52(3–4):1119–1127, August 1988. ISSN 1572-9613. doi:[10.1007/bf01019743](https://doi.org/10.1007/bf01019743). URL <http://dx.doi.org/10.1007/BF01019743>.

[21] Dieter A. Wolf-Gladrow. *Lattice Gas Cellular Automata and Lattice Boltzmann Models*. Springer Berlin Heidelberg, 2000. ISBN 9783540465867. doi:[10.1007/b72010](https://doi.org/10.1007/b72010). URL <http://dx.doi.org/10.1007/b72010>.

[22] P. H. Kourtz and W. G. O'Regan. A model a small forest fire ... to simulate burned and burning areas for use in a detection model. *Forest Science*, 17(2):163–169, 06 1971. ISSN 0015-749X. doi:[10.1093/forestscience/17.2.163](https://doi.org/10.1093/forestscience/17.2.163). URL <https://doi.org/10.1093/forestscience/17.2.163>.

[23] Per Bak, Kan Chen, and Chao Tang. A forest-fire model and some thoughts on turbulence. *Physics Letters A*, 147(5):297–300, 1990. ISSN 0375-9601. doi:[https://doi.org/10.1016/0375-9601\(90\)90451-S](https://doi.org/10.1016/0375-9601(90)90451-S). URL <https://www.sciencedirect.com/science/article/pii/037596019090451S>.

[24] B. Drossel and F. Schwabl. Self-organized critical forest-fire model. *Phys. Rev. Lett.*, 69:1629–1632, Sep 1992. doi:[10.1103/PhysRevLett.69.1629](https://doi.org/10.1103/PhysRevLett.69.1629). URL <https://link.aps.org/doi/10.1103/PhysRevLett.69.1629>.

[25] Kai Nagel and Michael Schreckenberg. A cellular automaton model for freeway traffic. *Journal de Physique I*, 2(12):2221–2229, December 1992. ISSN 1286-4862. doi:[10.1051/jp1:1992277](https://doi.org/10.1051/jp1:1992277). URL <http://dx.doi.org/10.1051/jp1:1992277>.

[26] Anasua Chakraborty, Sujit Sikder, Hichem Omrani, and Jacques Teller. Cellular automata in modeling and predicting urban densification: Revisiting the literature since 1971. *Land*, 11(7), 2022. ISSN 2073-445X. doi:[10.3390/land11071113](https://doi.org/10.3390/land11071113). URL <https://www.mdpi.com/2073-445X/11/7/1113>.

[27] S. Nandi, B.K. Kar, and P. Pal Chaudhuri. Theory and applications of cellular automata in cryptography. *IEEE Transactions on Computers*, 43(12):1346–1357, 1994. doi:[10.1109/12.338094](https://doi.org/10.1109/12.338094).

[28] Randall E. Rausch. The relationship between one-dimensional continuous cellular automata and one-dimensional nonlinear dynamical systems. *Complex Syst.*, 13(2), 2001. URL http://www.complex-systems.com/abstracts/v13_i02_a02.html.

[29] Bert Wang-Chak Chan. Lenia: Biology of artificial life. *Complex Systems*, 28(3):251–286, October 2019. ISSN 0891-2513. doi:[10.25088/complexsystems.28.3.251](https://doi.org/10.25088/complexsystems.28.3.251). URL <http://dx.doi.org/10.25088/ComplexSystems.28.3.251>.

[30] Alexander Mordvintsev, Ettore Randazzo, Eyyvind Niklasson, and Michael Levin. Growing neural cellular automata. *Distill*, 5(2), February 2020. ISSN 2476-0757. doi:[10.23915/distill.00023](https://doi.org/10.23915/distill.00023). URL <http://dx.doi.org/10.23915/distill.00023>.

[31] *Growing Isotropic Neural Cellular Automata*, volume ALIFE 2022: The 2022 Conference on Artificial Life of ALIFE 2022: The 2022 Conference on Artificial Life, 07 2022. doi:[10.1162/isal_a_00552](https://doi.org/10.1162/isal_a_00552). URL https://doi.org/10.1162/isal_a_00552.

[32] OpenAI, :, Aaron Hurst, Adam Lerer, Adam P. Goucher, Adam Perelman, Aditya Ramesh, Aidan Clark, AJ Ostrow, Akila Welihinda, Alan Hayes, Alec Radford, Aleksander Mądry, Alex Baker-Whitcomb, Alex Beutel, Alex Borzunov, Alex Carney, Alex Chow, Alex Kirillov, Alex Nichol, Alex Paino, Alex Renzin, Alex Tachard Passos, Alexander Kirillov, Alexi Christakis, Alexis Conneau, Ali Kamali, Allan Jabri, Allison Moyer, Allison Tam, Amadou Crookes, Amin Tootoochian, Amin Tootoonchian, Ananya Kumar, Andrea Vallone, Andrej Karpathy, Andrew Braunstein, Andrew Cann, Andrew Codispoti, Andrew Galu, Andrew Kondrich, Andrew Tulloch, Andrey Mishchenko, Angela Baek, Angela Jiang, Antoine Pelisse, Antonia Woodford, Anuj Gosalia, Arka Dhar, Ashley Pantuliano, Avi Nayak, Avital Oliver, Barret Zoph, Behrooz Ghorbani, Ben Leimberger, Ben Rossen, Ben Sokolowsky, Ben Wang, Benjamin Zweig, Beth Hoover, Blake Samic, Bob McGrew, Bobby Spero, Bogo Giertler, Bowen Cheng, Brad Lightcap, Brandon Walkin, Brendan Quinn, Brian Guaraci, Brian Hsu, Bright Kellogg, Brydon Eastman, Camillo Lugaressi, Carroll Wainwright, Cary Bassin, Cary Hudson, Casey Chu, Chad Nelson, Chak Li, Chan Jun Shern, Channing Conger, Charlotte Barette, Chelsea Voss, Chen Ding, Cheng Lu, Chong Zhang, Chris Beaumont, Chris Hallacy, Chris Koch, Christian Gibson, Christina Kim, Christine Choi, Christine McLeavey, Christopher Hesse, Claudia Fischer, Clemens Winter, Coley Czarnecki, Colin Jarvis, Colin Wei, Constantin Koumouzelis, Dane Sherburn, Daniel Kappler, Daniel Levin, Daniel Levy, David Carr, David Farhi, David Mely, David Robinson, David Sasaki, Denny Jin, Dev Valladares, Dimitris Tsipras, Doug Li, Duc Phong Nguyen, Duncan Findlay, Edede Oiwoh, Edmund Wong, Ehsan Asdar, Elizabeth Proehl, Elizabeth Yang, Eric Antonow, Eric Kramer, Eric Peterson, Eric Sigler, Eric Wallace, Eugene Brevdo, Evan Mays, Farzad Khorasani, Felipe Petroski Such, Filippo Raso, Francis Zhang, Fred von Lohmann, Freddie Sulit, Gabriel Goh, Gene Oden, Geoff Salmon, Giulio Starace, Greg Brockman, Hadi Salman, Haiming Bao, Haitang Hu, Hannah Wong, Haoyu Wang, Heather Schmidt, Heather Whitney, Heewoo Jun, Hendrik Kirchner, Henrique Ponde de Oliveira Pinto, Hongyu Ren, Huiwen Chang, Hyung Won Chung, Ian Kivlichan, Ian O'Connell, Ian O'Connell, Ian Osband, Ian Silber, Ian Sohl, Ibrahim Okuyucu, Ikai Lan, Ilya Kostrikov, Ilya Sutskever, Ingmar Kanitscheider, Ishaan Gulrajani, Jacob Coxon, Jacob Menick, Jakub Pachocki, James Aung, James Betker, James Crooks, James Lennon, Jamie Kiro, Jan Leike, Jane Park, Jason Kwon, Jason Phang, Jason Teplitz, Jason Wei, Jason Wolfe, Jay Chen, Jeff Harris, Jenia Varavva, Jessica Gan Lee, Jessica Shieh, Ji Lin, Jiahui Yu, Jiayi Weng, Jie Tang, Jieqi Yu, Joanne Jang, Joaquin Quinonero Candela, Joe Beutler, Joe Landers, Joel Parish, Johannes Heidecke, John Schulman, Jonathan Lachman, Jonathan McKay, Jonathan Uesato, Jonathan Ward, Jong Wook Kim, Joost Huizinga, Jordan Sitkin, Jos Kraaijeveld, Josh Gross, Josh Kaplan, Josh Snyder, Joshua Achiam, Joy Jiao, Joyce Lee, Juntang Zhuang, Justyn Harriman, Kai Fricke, Kai Hayashi, Karan Singhal, Katy Shi, Kavin Karthik, Kayla Wood, Kendra Rimbach, Kenny Hsu, Kenny Nguyen, Keren Gu-Lemberg, Kevin Button, Kevin Liu, Kiel Howe, Krithika Muthukumar, Kyle Luther, Lama Ahmad, Larry Kai, Lauren Itow, Lauren Workman, Leher Pathak, Leo Chen, Li Jing, Lia Guy, Liam Fedus, Liang Zhou, Lien Mamitsuka, Lilian Weng, Lindsay McCallum, Lindsey Held, Long Ouyang, Louis Feuvrier, Lu Zhang, Lukas Kondraciuk, Lukasz Kaiser, Luke Hewitt, Luke Metz, Lyric Doshi, Mada Aflak, Maddie Simens, Madelaine Boyd, Madeleine Thompson, Marat Dukhan, Mark Chen, Mark Gray, Mark Hudnall, Marvin Zhang, Marwan Aljubeh, Mateusz Litwin, Matthew Zeng, Max Johnson, Maya Shetty, Mayank Gupta, Meghan Shah, Mehmet Yatbaz, Meng Jia Yang, Mengchao Zhong, Mia Glaese, Mianna Chen, Michael Janner, Michael Lampe, Michael Petrov, Michael Wu, Michele Wang, Michelle Fradin, Michelle Pokrass, Miguel Castro, Miguel Oom Temudo de Castro, Mikhail Pavlov, Miles Brundage, Miles Wang, Minal Khan, Mira Murati, Mo Bavarian, Molly Lin, Murat Yesildal, Nacho Soto, Natalia Gimelshein, Natalie Cone, Natalie Staudacher, Natalie Summers, Natan LaFontaine, Neil Chowdhury, Nick Ryder, Nick Stathas, Nick Turley, Nik Tezak, Niko Felix, Nithanth Kudige, Nitish Keskar, Noah Deutsch, Noel Bundick, Nora Puckett, Ofir Nachum, Ola Okelola, Oleg Boiko, Oleg Murk, Oliver Jaffe, Olivia Watkins, Olivier Godement, Owen Campbell-Moore, Patrick Chao, Paul McMillan,

Pavel Belov, Peng Su, Peter Bak, Peter Bakkum, Peter Deng, Peter Dolan, Peter Hoeschele, Peter Welinder, Phil Tillet, Philip Pronin, Philippe Tillet, Prafulla Dharival, Qiming Yuan, Rachel Dias, Rachel Lim, Rahul Arora, Rajan Troll, Randall Lin, Rapha Gontijo Lopes, Raul Puri, Reah Miyara, Reimar Leike, Renaud Gaubert, Reza Zamani, Ricky Wang, Rob Donnelly, Rob Honsby, Rocky Smith, Rohan Sahai, Rohit Ramchandani, Romain Huet, Rory Carmichael, Rowan Zellers, Roy Chen, Ruby Chen, Ruslan Nigmatullin, Ryan Cheu, Saachi Jain, Sam Altman, Sam Schoenholz, Sam Toizer, Samuel Miserendino, Sandhini Agarwal, Sara Culver, Scott Ethersmith, Scott Gray, Sean Grove, Sean Metzger, Shamez Hermani, Shantanu Jain, Shengjia Zhao, Sherwin Wu, Shino Jomoto, Shirong Wu, Shuaiqi Xia, Sonia Phene, Spencer Papay, Srinivas Narayanan, Steve Coffey, Steve Lee, Stewart Hall, Suchir Balaji, Tal Broda, Tal Stramer, Tao Xu, Tarun Gogineni, Taya Christianson, Ted Sanders, Tejal Patwardhan, Thomas Cunningham, Thomas Degry, Thomas Dimson, Thomas Raoux, Thomas Shadwell, Tianhao Zheng, Todd Underwood, Todor Markov, Toki Sherbakov, Tom Rubin, Tom Stasi, Tomer Kaftan, Tristan Heywood, Troy Peterson, Tyce Walters, Tyna Eloundou, Valerie Qi, Veit Moeller, Vinnie Monaco, Vishal Kuo, Vlad Fomenko, Wayne Chang, Weiyi Zheng, Wenda Zhou, Wesam Manassra, Will Sheu, Wojciech Zaremba, Yash Patil, Yilei Qian, Yongjik Kim, Youlong Cheng, Yu Zhang, Yuchen He, Yuchen Zhang, Yujia Jin, Yunxing Dai, and Yury Malkov. Gpt-4o system card, 2024. URL <https://arxiv.org/abs/2410.21276>.

[33] Aaditya Singh, Adam Fry, Adam Perelman, Adam Tart, Adi Ganesh, Ahmed El-Kishky, Aidan McLaughlin, Aiden Low, AJ Ostrow, Akhila Ananthram, Akshay Nathan, Alan Luo, Alec Helyar, Aleksander Madry, Aleksandr Efremov, Aleksandra Spyra, Alex Baker-Whitcomb, Alex Beutel, Alex Karpenko, Alex Makelov, Alex Neitz, Alex Wei, Alexandra Barr, Alexandre Kirchmeyer, Alexey Ivanov, Alexi Christakis, Alistair Gillespie, Allison Tam, Ally Bennett, Alvin Wan, Alyssa Huang, Amy McDonald Sandjideh, Amy Yang, Ananya Kumar, Andre Saraiva, Andrea Vallone, Andrei Gheorghe, Andres Garcia Garcia, Andrew Braunstein, Andrew Liu, Andrew Schmidt, Andrey Mereskin, Andrey Mishchenko, Andy Applebaum, Andy Rogerson, Ann Rajan, Annie Wei, Anoop Kotha, Anubha Srivastava, Anushree Agrawal, Arun Vijayvergiya, Ashley Tyra, Ashvin Nair, Avi Nayak, Ben Eggers, Bessie Ji, Beth Hoover, Bill Chen, Blair Chen, Boaz Barak, Borys Minaiev, Botao Hao, Bowen Baker, Brad Lightcap, Brandon McKinzie, Brandon Wang, Brendan Quinn, Brian Fioca, Brian Hsu, Brian Yang, Brian Yu, Brian Zhang, Brittany Brenner, Callie Riggins Zetino, Cameron Raymond, Camillo Lugaresi, Carolina Paz, Cary Hudson, Cedric Whitney, Chak Li, Charles Chen, Charlotte Cole, Chelsea Voss, Chen Ding, Chen Shen, Chengdu Huang, Chris Colby, Chris Hallacy, Chris Koch, Chris Lu, Christina Kaplan, Christina Kim, CJ Minott-Henriques, Cliff Frey, Cody Yu, Coley Czarnecki, Colin Reid, Colin Wei, Cory Decareaux, Cristina Scheau, Cyril Zhang, Cyrus Forbes, Da Tang, Dakota Goldberg, Dan Roberts, Dana Palmie, Daniel Kappler, Daniel Levine, Daniel Wright, Dave Leo, David Lin, David Robinson, Declan Grabb, Derek Chen, Derek Lim, Derek Salama, Dibya Bhattacharjee, Dimitris Tsipras, Dinghua Li, Dingli Yu, DJ Strouse, Drew Williams, Dylan Hunn, Ed Bayes, Edwin Arbus, Ekin Akyurek, Elaine Ya Le, Elana Widmann, Eli Yani, Elizabeth Proehl, Enis Sert, Enoch Cheung, Eri Schwartz, Eric Han, Eric Jiang, Eric Mitchell, Eric Sigler, Eric Wallace, Erik Ritter, Erin Kavanaugh, Evan Mays, Evgenii Nikishin, Fangyuan Li, Felipe Petroski Such, Filipe de Avila Belbute Peres, Filippo Raso, Florent Bekerman, Foivos Tsimpourlas, Fotis Chantzis, Francis Song, Francis Zhang, Gaby Raila, Garrett McGrath, Gary Briggs, Gary Yang, Giambattista Parascandolo, Gildas Chabot, Grace Kim, Grace Zhao, Gregory Valiant, Guillaume Leclerc, Hadi Salman, Hanson Wang, Hao Sheng, Haoming Jiang, Haoyu Wang, Haozhun Jin, Harshit Sikchi, Heather Schmidt, Henry Aspegren, Honglin Chen, Huida Qiu, Hunter Lightman, Ian Covert, Ian Kivlichan, Ian Silber, Ian Sohl, Ibrahim Hammoud, Ignasi Clavera, Ikai Lan, Ilge Akkaya, Ilya Kostrikov, Irina Kofman, Isak Ettinger, Ishaan Singal, Jackie Hehir, Jacob Huh, Jacqueline Pan, Jake Wilczynski, Jakub Pachocki, James Lee, James Quinn, Jamie Kiro, Janvi Kalra, Jasmyn Samaroo, Jason Wang, Jason Wolfe, Jay Chen, Jay Wang, Jean Harb, Jeffrey Han, Jeffrey Wang, Jennifer Zhao, Jeremy Chen, Jerene Yang, Jerry Tworek, Jesse Chand, Jessica Landon, Jessica Liang, Ji Lin, Jiancheng Liu, Jianfeng Wang, Jie Tang, Jihan Yin, Joanne Jang, Joel Morris, Joey Flynn, Johannes Ferstad, Johannes Heidecke, John Fishbein, John Hallman, Jonah Grant, Jonathan Chien, Jonathan Gordon, Jongsoo Park, Jordan Liss, Jos Kraaijeveld, Joseph Guay, Joseph Mo, Josh Lawson, Josh McGrath, Joshua Vendrow, Joy Jiao, Julian Lee, Julie Steele, Julie Wang, Junhua Mao, Kai Chen, Kai Hayashi, Kai Xiao, Kamyar Salahi, Kan Wu, Karan Sekhri, Karan Sharma, Karan Singhal, Karen Li, Kenny Nguyen, Keren Gu-Lemberg, Kevin King, Kevin Liu, Kevin Stone, Kevin Yu, Kristen Ying, Kristian Georgiev, Kristie Lim, Kushal Tirumala, Kyle Miller, Lama Ahmad, Larry Lv, Laura Clare, Laurance Fauconnet, Lauren Itow, Lauren Yang, Laurentia Romaniuk, Leah Anise, Lee Byron, Leher Pathak, Leon Maksin, Leyan Lo, Leyton Ho, Li Jing, Liang Wu, Liang Xiong, Lien Mamitsuka, Lin Yang, Lindsay McCallum, Lindsey Held, Liz Bourgeois, Logan Engstrom, Lorenz Kuhn, Louis Feuvrier, Lu Zhang, Lucas Switzer, Lukas Kondraciuk, Lukasz Kaiser, Manas Joglekar, Mandeep Singh, Mandip Shah, Manuka Stratta, Marcus Williams, Mark Chen, Mark Sun, Marselus Cayton, Martin Li, Marvin Zhang, Marwan Aljubeh, Matt Nichols, Matthew Haines, Max Schwarzer, Mayank Gupta, Meghan Shah, Melody Huang, Meng Dong, Mengqing Wang, Mia Glaese, Micah Carroll, Michael Lampe, Michael Malek, Michael Sharman, Michael Zhang, Michele Wang, Michelle Pokrass, Mihai Florian, Mikhail Pavlov, Miles Wang, Ming Chen, Mingxuan Wang, Minnia Feng, Mo Bavarian, Molly Lin, Moose Abdool, Mostafa Rohaninejad, Nacho Soto, Natalie Staudacher, Natan LaFontaine, Nathan Marwell, Nelson Liu, Nick Preston, Nick Turley, Nicklas Anzman, Nicole Blades, Nikil Pancha, Nikita Mikhaylin, Niko Felix, Nikunj Handa, Nishant Rai, Nitish Keskar, Noam Brown, Ofir Nachum, Oleg Boiko, Oleg Murk, Olivia Watkins, Oona Gleeson, Pamela Mishkin, Patryk Lesiewicz, Paul Baltescu, Pavel Belov, Peter Zhokhov, Philip Pronin, Phillip Guo, Phoebe Thacker, Qi Liu, Qiming Yuan, Qinghua Liu, Rachel Dias, Rachel Puckett, Rahul Arora, Ravi Teja Mullapudi, Raz Gaon, Reah Miyara, Rennie Song, Rishabh Aggarwal, RJ Marsan, Robel Yemiru, Robert Xiong, Rohan Kshirsagar, Rohan Nuttall, Roman Tsliupa, Ronen Eldan, Rose Wang, Roshan James, Roy Ziv, Rui Shu, Ruslan Nigmatullin, Saachi Jain, Saam Talaie, Sam Altman, Sam Arnesen, Sam Toizer, Sam Toyer, Samuel Miserendino, Sandhini Agarwal, Sarah Yoo, Savannah Heon, Scott Ethersmith, Sean Grove, Sean Taylor, Sebastien Bubeck, Sever Banesi, Shaokyi Amdo, Shengjia Zhao, Sherwin Wu, Shibani Santurkar, Shiyu Zhao, Shraman Ray Chaudhuri, Shreyas Krishnaswamy, Shuaiqi Xia, Shuyang Cheng, Shyamal Anadkat, Simón Posada

Fishman, Simon Tobin, Siyuan Fu, Somay Jain, Song Mei, Sonya Egoian, Spencer Kim, Spug Golden, SQ Mah, Steph Lin, Stephen Imm, Steve Sharpe, Steve Yadlowsky, Sulman Choudhry, Sungwon Eum, Suvansh Sanjeev, Tabarak Khan, Tal Stramer, Tao Wang, Tao Xin, Tarun Gogineni, Taya Christianson, Ted Sanders, Tejal Patwardhan, Thomas Degry, Thomas Shadwell, Tianfu Fu, Tianshi Gao, Timur Garipov, Tina Sriskandarajah, Toki Sherbakov, Tomer Kaftan, Tomo Hiratsuka, Tongzhou Wang, Tony Song, Tony Zhao, Troy Peterson, Val Kharitonov, Victoria Chernova, Vineet Kosaraju, Vishal Kuo, Vitchyr Pong, Vivek Verma, Vlad Petrov, Wanning Jiang, Weixing Zhang, Wenda Zhou, Wenlei Xie, Wenting Zhan, Wes McCabe, Will DePue, Will Ellsworth, Wulfie Bain, Wyatt Thompson, Xiangning Chen, Xiangyu Qi, Xin Xiang, Xinwei Shi, Yann Dubois, Yaodong Yu, Yara Khakbaz, Yifan Wu, Yilei Qian, Yin Tat Lee, Yinbo Chen, Yizhen Zhang, Yizhong Xiong, Yonglong Tian, Young Cha, Yu Bai, Yu Yang, Yuan Yuan, Yuanzhi Li, Yufeng Zhang, Yuguang Yang, Yujia Jin, Yun Jiang, Yunyun Wang, Yushi Wang, Yutian Liu, Zach Stubenvoll, Zehao Dou, Zheng Wu, and Zhigang Wang. Openai gpt-5 system card, 2025. URL <https://arxiv.org/abs/2601.03267>.

[34] OpenAI. Models (openai api documentation). URL <https://developers.openai.com/api/docs/models>.

[35] Ines Montani, Matthew Honnibal, Matthew Honnibal, Adriane Boyd, Sofie Van Landeghem, and Henning Peters. spacy: Industrial-strength natural language processing in python, 2023. URL <https://zenodo.org/doi/10.5281/zenodo.1212303>.

[36] Note1. There was one case where “a” was matched; however, this was because spaCy incorrectly identified the article “a” in “... cell remains a pass ...” as a pronoun.

[37] Woosuk Kwon, Zhuohan Li, Siyuan Zhuang, Ying Sheng, Lianmin Zheng, Cody Hao Yu, Joseph E. Gonzalez, Hao Zhang, and Ion Stoica. Efficient memory management for large language model serving with pagedattention, 2023. URL <https://arxiv.org/abs/2309.06180>.

[38] Lianmin Zheng, Liangsheng Yin, Zhiqiang Xie, Chuyue Sun, Jeff Huang, Cody Hao Yu, Shiyi Cao, Christos Kozyrakis, Ion Stoica, Joseph E. Gonzalez, Clark Barrett, and Ying Sheng. Sglang: Efficient execution of structured language model programs, 2024. URL <https://arxiv.org/abs/2312.07104>.

Appendix A: ALife: Temporal Evolution and Clustering

1. GPT-5-nano

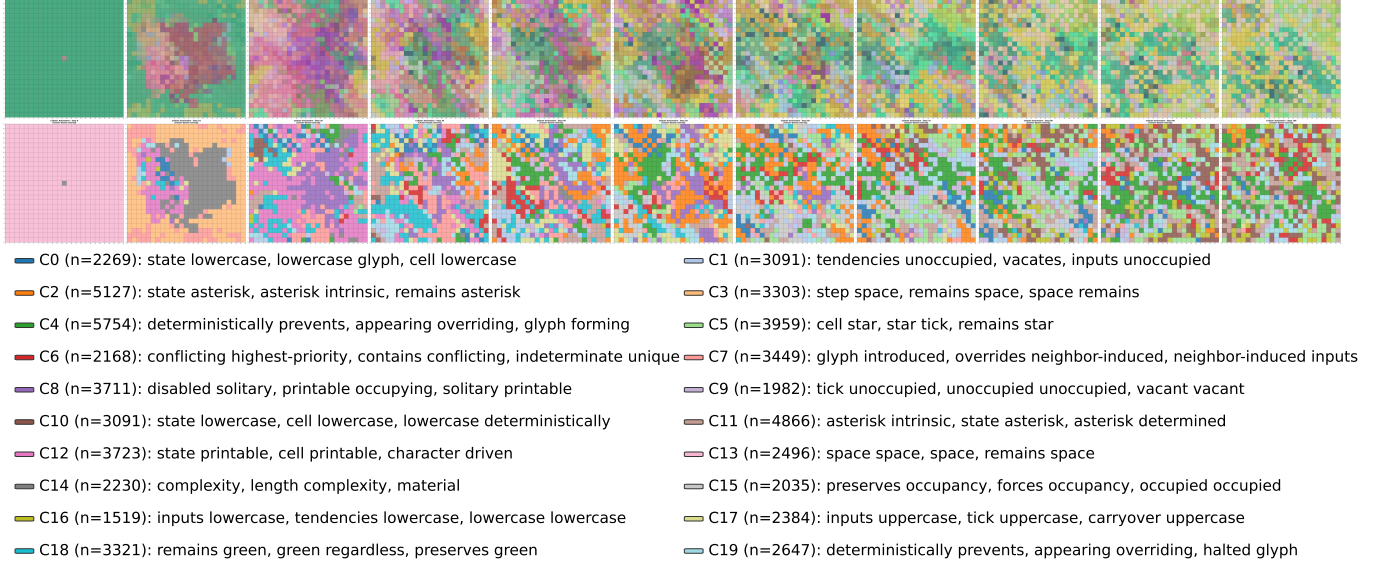


FIG. 6: Results of Run 2 for GPT-5-nano in the ALife experiment. The top row shows the Global color space and the bottom row shows the cluster-based visualization. See Fig. 2 for details.

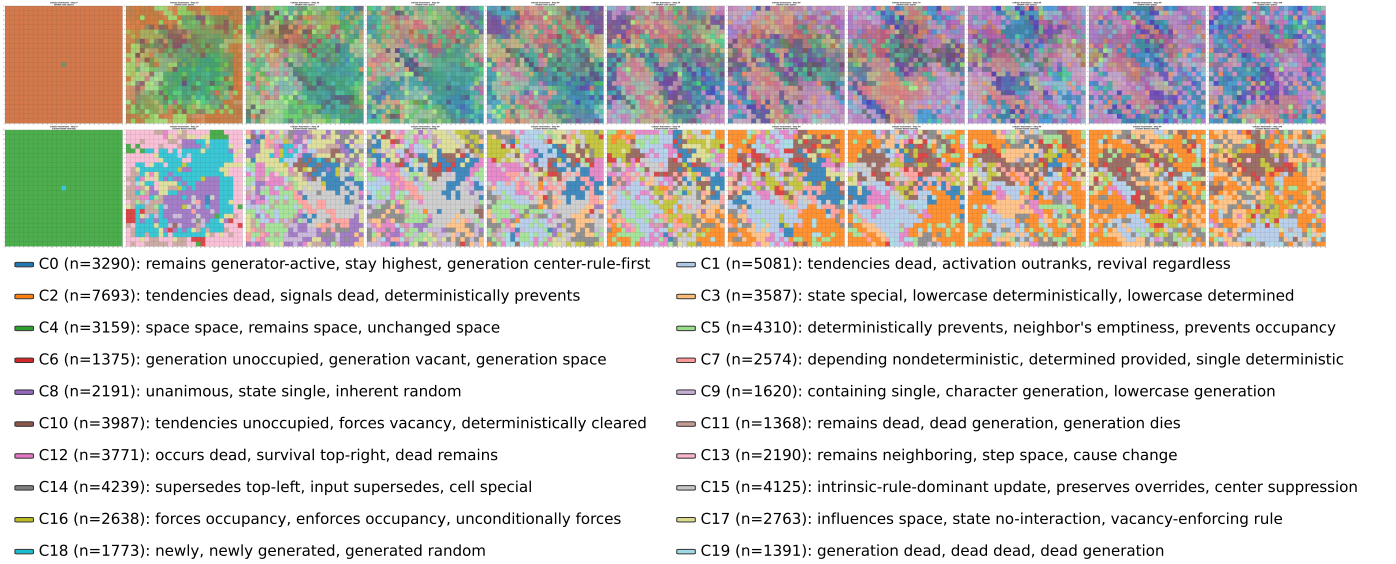


FIG. 7: Results of Run 3 for GPT-5-nano in the ALife experiment. The top row shows the Global color space and the bottom row shows the cluster-based visualization. See Fig. 2 for details.

2. GPT-5-mini

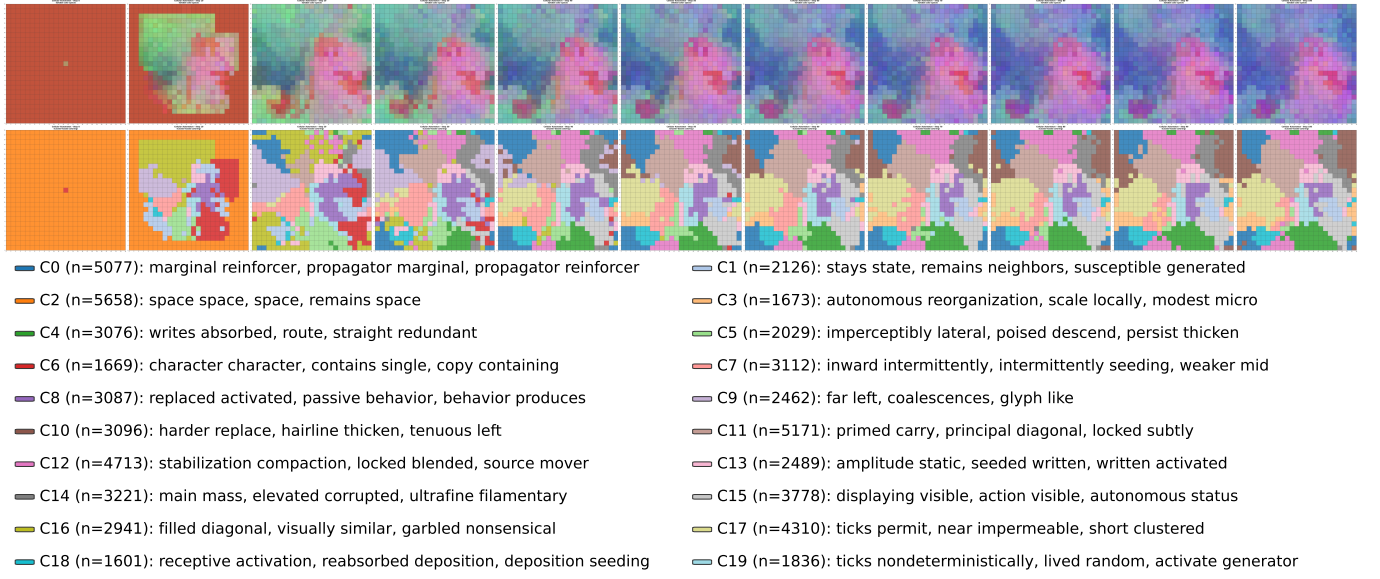


FIG. 8: Results of Run 2 for GPT-5-mini in the ALife experiment. The top row shows the Global color space and the bottom row shows the cluster-based visualization. See Fig. 3 for details.

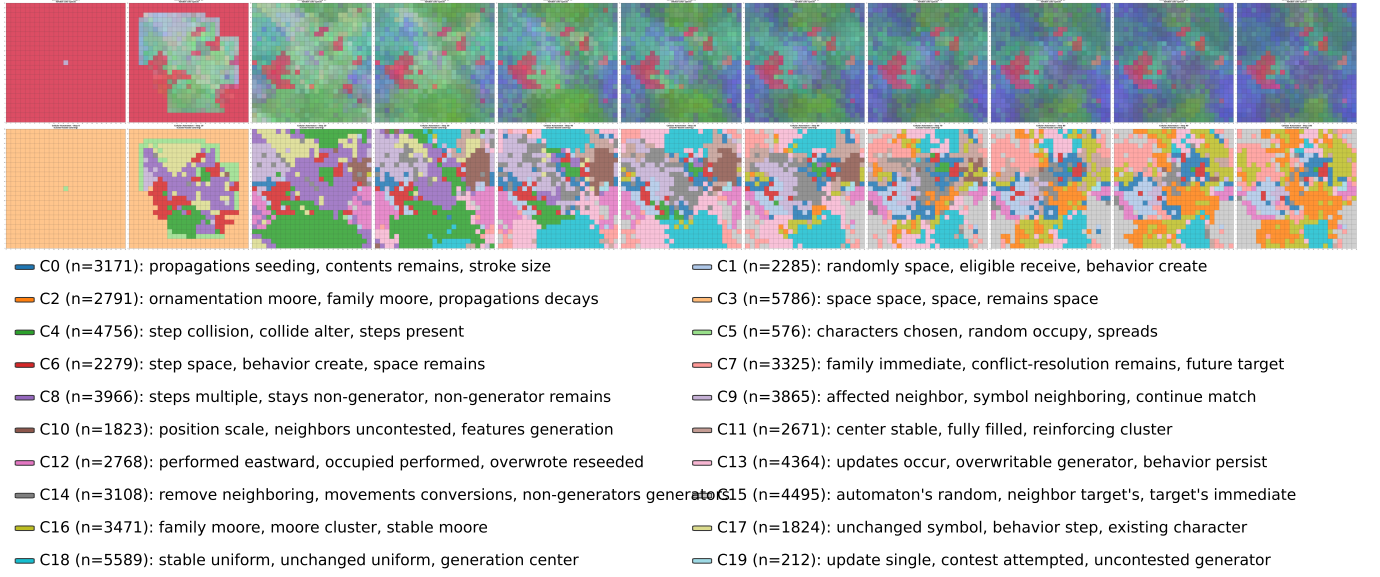


FIG. 9: Results of Run 3 for GPT-5-mini in the ALife experiment. The top row shows the Global color space and the bottom row shows the cluster-based visualization. See Fig. 3 for details.